Acta Crystallographica Section F
Structural Biology and Crystallization Communications
ISSN 1744-3091

Preliminary neutron and X-ray crystallographic studies of equine cyanomethemoglobin

A. Y. Kovalevsky,[a] S. Zoe Fisher,[a] Sean Seaver,[b] Marat Mustyakimov,[a] Narayanasami Sukumar,[c] Paul Langan,[a,b] Timothy C. Mueser[b] and B. Leif Hanson[b]*

[a]Bioscience Division, MS M888, Los Alamos National Laboratory, Los Alamos, NM 87545, USA, [b]Department of Chemistry, University of Toledo, Toledo, OH 43606, USA, and [c]NE-CAT, APS, Argonne National Laboratory, Argonne, IL 60439, USA

Correspondence e-mail: leif.hanson@gmail.com

Received 9 December 2009
Accepted 1 March 2010

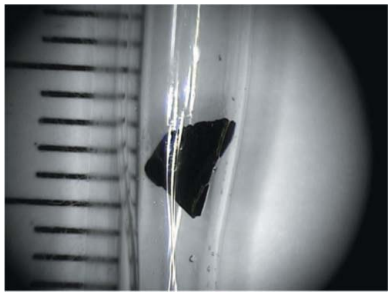

Room-temperature and 100 K X-ray and room-temperature neutron diffraction data have been measured from equine cyanomethemoglobin to 1.7 Å resolution using a home source, to 1.6 Å resolution on NE-CAT at the Advanced Photon Source and to 2.0 Å resolution on the PCS at Los Alamos Neutron Science Center, respectively. The cyanomethemoglobin is in the R state and preliminary room-temperature electron and neutron scattering density maps clearly show the protonation states of potential Bohr groups. Interestingly, a water molecule that is in the vicinity of the heme group and coordinated to the distal histidine appears to be expelled from this site in the low-temperature structure.

1. Introduction

Although X-ray crystallography is by far the pre-eminent method for determining protein structures, it has a fundamental limitation in determining the protonation states of amino-acid residues and the orientations of solvent molecules in the hydration shells of proteins, especially at moderate resolutions and ambient temperatures. The H atom scatters X-ray photons feebly, while H^+ is not visible to X-rays. In sharp contrast, the nucleus of the hydrogen isotope deuterium scatters neutrons as well as carbon and oxygen and almost as well as nitrogen. As a consequence, neutron protein crystallography continues to advance as a complementary experimental structure-interrogation technique owing to its unsurpassed power in the direct determination of hydrogen positions. Provided that most H atoms in the protein molecule are exchanged for D atoms prior to the neutron diffraction experiment, in a neutron protein structure the positions of D atoms are readily revealed at resolutions of 2.2 Å or better (Niimura & Bau, 2008). The knowledge of protonation states and hydration in proteins is indispensible for deeper understanding of how they function and in determining enzyme mechanisms.

Enzymes are not the only proteins for which investigations of the structure–function relationship can benefit from experimental determination of hydrogen positions. Hemoglobin, which is arguably one of the most well studied proteins, has eluded neutron studies for a long time owing to the size of its unit cell and the extended time needed to measure a full data set from a monoclinic cell. However, because of improvements in instrumentation and sample-preparation methods for neutron crystallography (Blakeley *et al.*, 2008), Chatake and coworkers were recently able to collect a 2.1 Å resolution neutron data set from human hemoglobin in the T state. The resulting information on the protonation states of residues provided some unique insights into the Bohr effect in human hemoglobin and raised some intriguing questions (Chatake *et al.*, 2007).

A 65 kDa tetramer composed of two $\alpha\beta$ heterodimer subunits, hemoglobin is reliant on His side chains for hydrogen-ion buffering, blood CO_2-transport capacity and the molecular mechanism for the reduced affinity for oxygen at low pH (or Bohr effect). The contribution of His side chains to the Bohr effect is still not fully resolved. Early studies by Perutz (1983) suggested a limited number of Bohr groups that are essentially conserved in vertebrate hemoglobins. However, more recent NMR work has suggested that a larger number of His side chains contribute to the Bohr effect (Lukin & Ho, 2004; Berenbrink, 2006). In addition, solvent motion and displacement mediate quaternary-stucture changes in hemoglobin. In the transition

from deoxygenated to oxygenated conditions [classically labelled the tense (T) and relaxed (R) states, respectively] there is now clear evidence that the dimer–dimer interface of liganded hemoglobin has a wide range of energetically accessible structures that are related to each other by a simple sliding motion (Mueser *et al.*, 2000). The dimer–dimer interface acts as a 'molecular slide bearing' that allows the two dimers to slide back and forth without greatly altering the number or the nature of the intersubunit contacts. Solvent plays an essential role in this interface sliding (Mueser *et al.*, 2000) and the mediation of T–R interconversion. The role of His side chains in the Bohr effect can be understood as either a limited number of side chains providing strong links to stabilize the T state (the Perutz model) or the aggregative and concerted effect of His-residue protonation stabilizing the T state (the Lukin and Ho model). In either case, knowledge of hydrogen positions and protonation states is essential to understanding the hemoglobin function.

To elucidate these issues, we are using neutrons to study the protonation states and hydration in the R state of equine hemoglobin. We have chosen equine hemoglobin because it is readily available and the R state of the protein forms large block crystals with moderate unit-cell edges that are well suited to neutron diffraction (Fig. 1). The information provided in this study on the protonation states of Bohr groups in the R state of equine hemoglobin might also be usefully compared with the information recently provided on their protonation in the T state of human hemoglobin (Chatake *et al.*, 2007). The cyanomet form of the protein was used because it proved to be more stable and easier to handle than the carbonmonoxy form. Both forms crystallize in isomorphous unit cells and have the same state of the hemoglobin tetramer (Mueser *et al.*, 2000).

Here, we report a neutron study in which the Protein Crystallography Station (PCS) built at the spallation neutron source run by Los Alamos Neutron Scattering Center (LANSCE) at Los Alamos National Laboratory (LANL) (Langan *et al.*, 2004) was used to obtain a complete data set from an equine cyanomethemoglobin (eqCNmetHb) crystal. The PCS has produced >80% complete data sets even for low-symmetry crystals (*e.g.* monoclinic) by using the time-of-flight (TOF) technique with spallation neutrons to measure three-dimensional diffraction images (Kovalevsky *et al.*, 2008; Fisher *et al.*, 2009; Tuan *et al.*, 2007). To further facilitate full data measurement, the PCS utilizes a large cylindrical neutron detector and a κ-circle goniometer. For these studies, we also collected room-temperature (293 K) and 100 K X-ray diffraction data sets utilizing a home source and a synchrotron, respectively. These are the first published diffraction studies to be performed on equine cyanomethemoglobin.

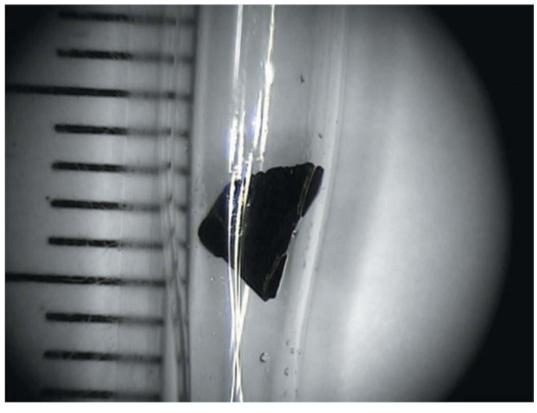

Figure 1
The crystal of equine cyanomethemoglobin used for the neutron diffraction data collection. The crystal measured about 3.5 × 2.5 × 1.2 mm in size (∼10 mm^3) and was mounted in an hourglass-shaped quartz capillary.

2. Crystallization

Equine hemoglobin was prepared as described previously (Perutz, 1968; Mueser *et al.*, 2000). Purified protein was oxidized to the ferric form and liganded with cyanide using 0.1 ml ferricyanide solution {20 m*M* $K_3[Fe(CN)_6]$, 20 m*M* NaCN, 10 m*M* HEPES pH 7.2} per millilitre of protein solution. The product eqCNmetHb was further purified on a desalting column (Sephadex G25; GE Healthcare) using 10 m*M* HEPES pH 7.2 and was concentrated to 40 mg ml^{-1} (the concentration in mg ml^{-1} was calculated as $A_{540\,\mathrm{nm}} \times 1.465$; International Committee for Standardization in Haematology, 1978). Crystallization of cyanomethemoglobin was carried out in H_2O according to the batch method. Crystallization drops of 500–800 µl volume were set up in a nine-well glass plate (Hampton Research) sealed airtight with CrystalClear tape (Hampton Research). Crystals of the order of 5–10 mm^3 in volume normally grew within a month at 290 K from drops containing 5 m*M* HEPES, 20 mg ml^{-1} eqCNmetHb and 40% saturated ammonium sulfate adjusted to pH 7.2 with NaOH (Fig. 1).

3. Data collection and reduction

3.1. Neutron crystallography

Several candidate crystals were successfully mounted in quartz capillaries (Fig. 1) that had been reshaped with a CH_4/O_2 torch to give an hourglass constriction to prevent the crystal from slipping during the diffraction experiment. Deuterated buffer (∼0.5 ml) was placed in the lower part of the capillary. H/D vapor exchange was allowed to occur in the capillary for one month before the collection of neutron diffraction data. A 17 h test exposure was taken from the largest eqCNmetHb crystal (∼10 mm^3), depicted in Fig. 1, yielding diffraction to better than 2.0 Å resolution. The diffraction quality and signal-to-noise ratio were deemed to be suitable for full data-set collection (Fig. 2).

Time-of-flight wavelength-resolved Laue images were collected at room temperature on a Huber κ-circle goniometer at 37 usable settings, with approximately 17 h exposure times per diffraction image (Fig. 2). The crystal-to-detector distance was set to 730 mm, corresponding to the cylindrical radius of the detector, while the detector was normally kept at $2\theta = 0^\circ$ during the entire experiment, effectively collecting data in the $\pm 60^\circ$ 2θ range. Because of the narrow $\pm 8^\circ$ span of the detector in the vertical direction the crystal had to be reoriented eight times using the κ and ω goniometer circles and φ scans performed at each crystal orientation. Each image was processed using a version of *d*TREK* (Pflugrath, 1999) modified for wavelength-resolved Laue neutron protein crystallography (Langan & Greene, 2004). The integrated reflections were wavelength-normalized using *LAUENORM* (Helliwell *et al.*, 1989) and merged

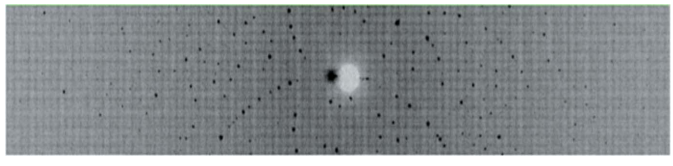

Figure 2
Neutron Laue diffraction pattern for the eqCNmetHb crystal. In the crystal setting the three-dimensional diffraction data were projected in time-of-flight to produce a conventional two-dimensional Laue pattern.

using *SCALA* incorporated into the *CCP*4 program suite (Evans, 2006; Weiss, 2001; Diederichs & Karplus, 1997; Weiss & Hilgenfeld, 1997; Collaborative Computational Project, Number 4, 1994). The 'tails' of the wavelength range were cut off slightly, with a restricted range of 0.72–6.25 Å, from the original 0.6–7.0 Å wavelength distribution of the thermal neutrons to eliminate the least accurately measured reflections. The overall completeness was 80.2% to 2.0 Å, with an $R_{\rm merge}$ of ∼24.2% and a redundancy of 2.7 for the low-symmetry space group *C*2.

Joint X-ray–neutron (XN) refinement of the structure is in progress utilizing the program *nCNS* (Adams *et al.*, 2009) modified from the original *CNS* (Brünger *et al.*, 1998) and including both 293 K neutron and 293 K X-ray reflection files in the refinement. Initial neutron-density maps (Fig. 3) calculated after rigid-body refinement and one round of positional and *B*-factor refinement show the clear features that are usually observed for neutron maps. D atoms on exchangeable groups such as OH and NH are clearly visible as strong nuclear density peaks. H atoms that are attached to non-exchangeable aliphatic and aromatic groups and have a negative scattering length for neutrons are detected as troughs in the negative $2F_{\rm o} - F_{\rm c}$ nuclear density map. Determination of protonation states and hydration will be performed during the XN refinement and reported elsewhere.

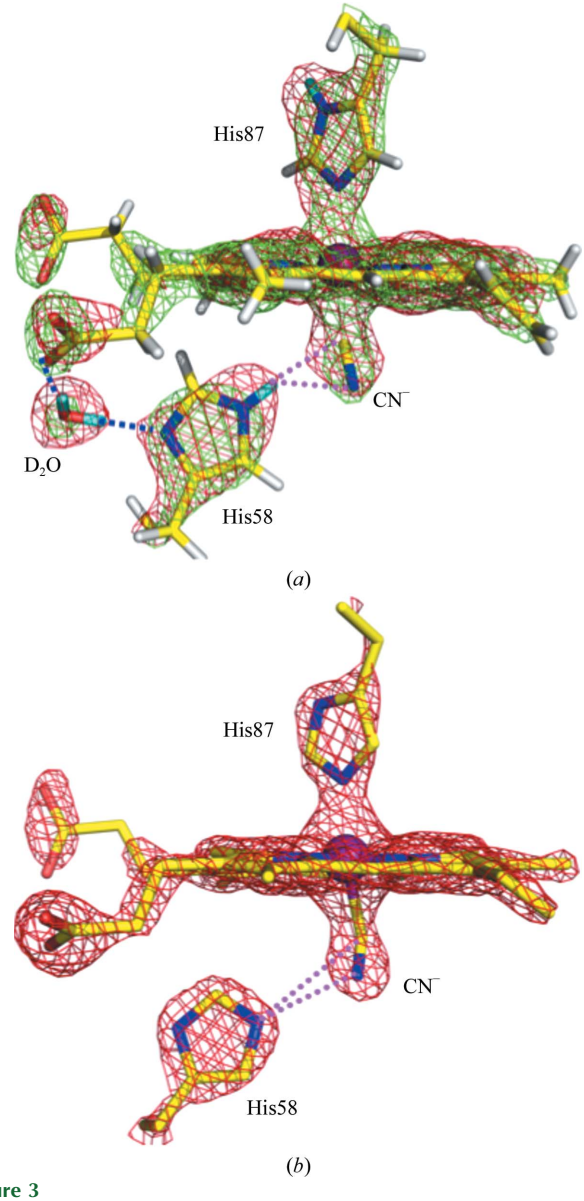

Figure 3
(*a*) Preliminary $2F_{\rm o} - F_{\rm c}$ nuclear density (red, contoured at the 2.2σ level) and electron-density (green, contoured at the 2.4σ level) maps calculated from room-temperature neutron diffraction and X-ray diffraction data, respectively. The heme and surrounding region of the α chain are shown. D atoms are colored cyan. Hydrogen bonds made by D_2O are represented as blue dashed lines, while the N—D···π contact between His58 and the cyanide ligand is shown as magenta dotted lines. (*b*) Preliminary $2F_{\rm o} - F_{\rm c}$ electron density contoured at the 2.5σ level for the same α-chain region calculated from 100 K X-ray diffraction data. Note the missing water between the C—O of the heme and His58.

Table 1
Room-temperature neutron diffraction data-collection statistics.

Values in parentheses are for the highest resolution shell.

Source	PCS, LANSCE, Los Alamos National Laboratory
Settings	37
Space group	*C*2
Unit-cell parameters (Å, °)	a = 108.86, b = 63.16, c = 54.71, β = 110.75
Unit-cell volume (Å^3)	351200
Resolution	21.58–2.00 (2.11–2.00)
No. of reflections (measured/unique)	51389/18780
Redundancy	2.7 (1.9)
Completeness (%)	80.2 (67.9)
$R_{\rm merge}$	0.242 (0.356)
$R_{\rm p.i.m.}$	0.163 (0.283)
Wavelength range (Å)	0.72–6.25
Mean (I)/sd	3.5 (1.4)

Table 2
X-ray diffraction data-collection statistics.

	293 K	100 K
Wavelength (Å)	1.5418 (Cu $K\alpha$)	1.00 (APS, NECAT)
Space group	*C*2	*C*2
Unit-cell parameters (Å, °)	a = 108.86, b = 63.16, c = 54.71, β = 110.7	a = 107.60, b = 62.97, c = 53.70, β = 111.48
Resolution (Å)	31.58–1.70 (1.76–1.70)	50.00–1.60 (1.66–1.60)
No. of reflections measured	137874	216212
Unique reflections	36049 (3351)	42939 (4141)
Redundancy	3.82 (3.77)	5.0 (4.8)
Completeness (%)	94.3 (90.8)	97.2 (94.2)
$\langle I/\sigma(I)\rangle$	10.9 (2.1)	18.9 (1.9)
$R_{\rm merge}$†	0.058 (0.348)	0.076 (0.565)

† $R_{\rm merge} = \sum_{hkl}\sum_i |I_i(hkl) - \langle I(hkl)\rangle| / \sum_{hkl}\sum_i I_i(hkl)$.

3.2. X-ray crystallography

The 293 K X-ray crystallographic data set was collected to 1.7 Å resolution in-house from a crystal of eqCNmetHb sealed in a thin-walled quartz capillary with D_2O buffer using a Rigaku FR-E diffractometer equipped with an R-AXIS IV^{++} detector. Diffraction data were integrated and scaled using the *CrystalClear*/*d***TREK* software (Pflugrath, 1999) and structure refinement is in progress using *SHELX* (Sheldrick, 2008). When using joint XN strategies for structure refinement it is essential that the X-ray and neutron data have been collected from isomorphous crystals. In order to ensure this, the crystals for both studies were taken from the same crystallization batch experiment and sealed in capillaries with identical D_2O buffer. The 100 K X-ray data set was collected to 1.6 Å resolution at a synchrotron from a small crystal frozen using the mother liquor as the cryoprotectant. A summary of the crystallographic data is given in Tables 1 and 2.

4. Discussion

To our knowledge, this is the first reported crystallographic study of equine cyanomethemoglobin. The crystals used in this study were grown under high-salt conditions (ammonium sulfate) at pH 7.2. Small crystals were chosen for 293 and 100 K X-ray diffraction data collection, while a large $\sim$10 mm^3 crystal was selected for a room-temperature neutron diffraction experiment at PCS. EqCNmetHb crystallized in space group $C2$ with one $\alpha\beta$ heterodimer in the asymmetric unit. Notably, the eqCNmetHb crystal was isomorphous to the previously reported carbonmonoxy derivative of equine hemoglobin (PDB code 1g0b; Mueser *et al.*, 2000) and adopts the classical high-salt R quaternary structure.

We obtained full X-ray data sets to 1.7 and 1.6 Å resolution at room and low temperature, respectively. Neutron diffraction data collection is in progress and we expect to collect a complete reflection set to 2 Å resolution. Preliminary electron-density and nuclear density maps for the heme groups and surrounding residues are depicted in Fig. 3, showing the heme iron coordination, D atoms on the proximal and distal His residues and a D_2O molecule hydrogen bonded to His58 for the room-temperature data. At 100 K this water molecule appears to be expelled from the site. The current neutron structure represents the relaxed quaternary state of hemoglobin, which has high oxygen affinity and an altered tertiary structure compared with that of T-state hemoglobin. Our hope is that comparison of this structure with that of deoxy human hemoglobin (Chatake *et al.*, 2007) will prove to be useful in detecting differences in the protonation states of histidine residues that change their charge state during the T–R transition (Berenbrink, 2006).

The PCS is funded by the Office of Biological and Environmental Research of the US Department of Energy. MM and PL were partly supported by an NIH–NIGMS-funded consortium (1R01GM071939-01) between LANL and LBNL to develop computational tools for neutron protein crystallography. AYK was partly supported by an LANL LDRD grant (20080789PRD3). AYK and PL were partly supported by an LANL LDRD grant (20070131ER). TCM and BLH were supported by NSF (446218). This work is based upon research conducted at the Advanced Photon Source on the Northeastern Collaborative Access Team beamlines, which are supported by award RR-15301 from the National Center for Research Resources at the National Institutes of Health. Use of the Advanced Photon Source is supported by the US Department of Energy, Office of Basic Energy Sciences under Contract No. DE-AC02-06CH11357.

References

Adams, P. D., Mustyakimov, M., Afonine, P. V. & Langan, P. (2009). *Acta Cryst.* D**65**, 567–573.
Berenbrink, M. (2006). *Resp. Physiol. Neurobiol.* **154**, 165–184.
Blakeley, M., Langan, P., Niimura, N. & Podjarny, A. (2008). *Curr. Opin. Struct. Biol.* **18**, 593–600.
Brünger, A. T., Adams, P. D., Clore, G. M., DeLano, W. L., Gros, P., Grosse-Kunstleve, R. W., Jiang, J.-S., Kuszewski, J., Nilges, M., Pannu, N. S., Read, R. J., Rice, L. M., Simonson, T. & Warren, G. L. (1998). *Acta Cryst.* D**54**, 905–921.
Chatake, T., Shibayama, N., Park, S.-H. Y., Kurihara, K., Tamada, T., Tanaka, I., Niimura, N., Kuroki, R. & Morimoto, Y. (2007). *J. Am. Chem. Soc.* **129**, 14840–14841.
Collaborative Computational Project, Number 4 (1994). *Acta Cryst.* D**50**, 760–763.
Diederichs, K. & Karplus, P. A. (1997). *Nature Struct. Biol.* **4**, 269–275.
Evans, P. (2006). *Acta Cryst.* D**62**, 72–82.
Fisher, S. Z., Kovalevsky, A. Y., Domsic, J. F., Mustyakimov, M., Silverman, D. N., McKenna, R. & Langan, P. (2009). *Acta Cryst.* F**65**, 495–498.
Helliwell, J. R., Habash, J., Cruickshank, D. W. J., Harding, M. M., Greenhough, T. J., Campbell, J. W., Clifton, I. J., Elder, M., Machin, P. A., Papiz, M. Z. & Zurek, S. (1989). *J. Appl. Cryst.* **22**, 483–497.
International Committee for Standardization in Haematology (1978). *J. Clin. Pathol.* **31**, 139–143.
Kovalevsky, A. Y., Chatake, T., Shibayama, N., Park, S.-Y., Ishikawa, T., Mustyakimov, M., Fisher, S. Z., Langan, P. & Morimoto, Y. (2008). *Acta Cryst.* F**64**, 270–273.
Langan, P. & Greene, G. (2004). *J. Appl. Cryst.* **37**, 253–257.
Langan, P., Greene, G. & Schoenborn, B. P. (2004). *J. Appl. Cryst.* **37**, 24–31.
Lukin, J. A. & Ho, C. (2004). *Chem. Rev.* **104**, 1219–1230.
Mueser, T. C., Rogers, P. H. & Arnone, A. (2000). *Biochemistry*, **39**, 15353–15364.
Niimura, N. & Bau, R. (2008). *Acta Cryst.* A**64**, 12–22.
Perutz, M. F. (1968). *J. Cryst. Growth*, **2**, 54–56.
Perutz, M. F. (1983). *Mol. Biol. Evol.* **1**, 1–28.
Pflugrath, J. W. (1999). *Acta Cryst.* D**55**, 1718–1725.
Sheldrick, G. M. (2008). *Acta Cryst.* A**64**, 112–122.
Tuan, H.-F., Erskine, P., Langan, P., Cooper, J. & Coates, L. (2007). *Acta Cryst.* F**63**, 1080–1083.
Weiss, M. S. (2001). *J. Appl. Cryst.* **34**, 130–135.
Weiss, M. S. & Hilgenfeld, R. (1997). *J. Appl. Cryst.* **30**, 203–205.